Heliyon 10 (2024) e33936

Contents lists available at ScienceDirect

Heliyon

journal homepage: www.cell.com/heliyon

Research article

# Celastrol induces ferroptosis by suppressing RRM2 in hepatocellular carcinoma

Xue Zhang [a,b,1], Manman Qi [c,1], Kailun Huo [d,1], Banglan Cai [a,b], Jian Zhang [e,**], Yijun Tian [f,***], Denghai Zhang [b,*]

[a] Ningxia Medical University School of Basic Medical Sciences, Yinchuan, 750004, China
[b] Shanghai Health Commission Key Lab of Artificial Intelligence (AI)-Based Management of Inflammation and Chronic Diseases, Sino-French Cooperative Central Lab, Shanghai Pudong Gongli Hospital, Shanghai, 200135, China
[c] Shanghai University School of Medicine, Shanghai, 200444, China
[d] Postgraduate Training Base at Shanghai Pudong Gongli Hospital, Ningxia Medical University, Yinchuan, 750004, China
[e] Shanghai Universal Medical Imaging Diagnostic Center, Shanghai University, Shanghai, 200030, China
[f] Department of Urology, Tongji Hospital, School of Medicine, Tongji University, Shanghai, 200065, China

ARTICLE INFO

*Keywords:*
Ferroptosis
Celastrol
RRM2
HCC
Traditional Chinese medicine

ABSTRACT

*Introduction and Objectives:* Ferroptosis is a novel form of cell death driven by iron dependence and lipid peroxidation, presenting a promising potential as an innovative strategy for cancer treatment. Celastrol (Cel) is particularly effective in inducing ferroptosis, but its molecular mechanism remains unclear. The study aims to elucidate the potential mechanism through both in vitro and in vivo experiments.

*Materials and methods:* CCK-8 assay, Western blot analysis and measurements of reactive oxygen species (ROS), malondialdehyde (MDA), and glutathione (GSH) were performed to investigate how Cel inhibits the proliferation of hepatocellular carcinoma (HCC) cells via the ferroptosis mechanism. Bioinformatics analysis based on the TCGA-LIHC and FerrDb databases was performed to identify the target gene RRM2, and molecular docking-simulated binding between RRM2 and Cel. The role of RRM2 in the effects of Cel was determined through lentiviral transfection, Transwell assays, and in vivo experiments.

*Results:* Cel inhibited HCC cell proliferation via the ferroptosis pathway. Inhibition RRM2 significantly reduces mTOR protein phosphorylation, while overexpressing RRM2 can attenuate theeffects of Cel on the proliferation, migration, invasion, and ferroptosis induction of HCC cells. The result of in vivo experiments in nude mice demonstrated that Cel inhibited tumor growth

*Abbreviations:* Cel, celastrol; HCC, hepatocellular carcinoma; RRM2, Ribonucleotide Reductase M2; DMEM, Dulbecco's Modified Eagle Medium; CCK-8, Cell Counting Kit-8; NAC, N-acetylcysteine; DFO, deferoxamine; ROS, Reactive oxygen species; MDA, Malondialdehyde; GSH-Px, Glutathione Peroxidase; GEO, Gene Expression Omnibus; TCGA, The Cancer Genome Atlas; LIHC, liver hepatocellular carcinoma; CTD, Comparative Toxicogenomics Database; DEGs, Differentially Expressed Genes; PPI, Protein-Protein Interaction; OS, Overall Survival; PFS, Progression-free Survival; ROC, Receiver Operating Characteristic; AUC, Area Under the Curve; GSEA, Gene Set Enrichment Analysis; EdU, 5-ethynyl-2′-deoxyuridine; DMSO, Dimethyl Sulfoxide; AST, Aspartate Aminotransferase; ALT, Alanine Aminotransferase; Cr, Creatinine; UA, Uric Acid; T-BIL, Total Bilirubin; LDH, Lactate Dehydrogenase; IHC, Immunohistochemistry; HE, Hematoxylin and Eosin.

* Corresponding author.
** Corresponding author.
*** Corresponding author.
*E-mail addresses:* abiaoxp@163.com (J. Zhang), balancesy@163.com (Y. Tian), Denghai_zhang@163.com (D. Zhang).
[1] Co-first authors.

https://doi.org/10.1016/j.heliyon.2024.e33936
Received 20 April 2024; Received in revised form 28 June 2024; Accepted 1 July 2024
Available online 2 July 2024

without adversely affecting liver and kidney function indicators. Immunohistochemistry and Western blot analyses revealed that Cel activated the key proteins in the ferroptosis pathway and affected crucial indicators such as malondialdehyde (MDA) and glutathione (GSH).
*Conclusion:* In this study, we clarifiy the molecular mechanism of Cel, thus broadening its clinical applications for treating various cancer types, including liver cancer.

## 1. Introduction

Hepatocellular carcinoma (HCC) represents a major global health challenge, being the sixth most common cancer worldwide, with especially high prevalence in Asia and sub-Saharan Africa [1,2]. For eligible patients, surgical interventions, primarily hepatectomy, offer the main curative approach [2,3]. Concurrently, pharmacotherapeutic strategies, encompassing systemic chemotherapy and molecular targeted therapies play a pivotal role in the management of this formidable malignancy [4].

Ferroptosis is a new type of programmed cell death, distinct from traditional ap. Ferroptosis has a different pathogenesis compared to apoptosis and necrosis. Apoptosis, another form of programmed cell death, operates through pathways involving caspase enzymes and mitochondrial signaling [5]. In contrast, necrosis is an unprogrammed form of cell death typically resulting from acute injury, leading to cell membrane rupture and leakage of cellular contents [6]. Many tumor cells exhibit higher sensitivity to ferroptosis due to their high metabolic rates and oxidative stress levels [7]. Therefore, investigating the relationship between ferroptosis and tumors not only helps to elucidate the diversity and complexity of tumor cell death but also offers new approaches and strategies for cancer treatment.

Celastrol, a triterpenoid compound extracted from Tripterygium wilfordii, has garnered significant attention for its remarkable anti-tumor activity [7,8]. Recent studies have shown that Celastrol can induce ferroptosis. Under Celastrol's influence, intracellular iron metabolism is altered, leading to an increase in iron ions [9]. These iron ions can catalyze lipid peroxidation, generating a large number of reactive oxygen species (ROS) [10]. These ROS can cause lipid peroxidation of the cell membrane, resulting in the destruction of membrane structure and ultimately leading to cell death. Renowned for its pivotal role in nucleotide metabolism, ribonucleotide reductase M2 (RRM2) is a critical enzyme contributing to DNA synthesis and repair [11,12]. In recent years, mounting evidence has underscored the multifaceted involvement of RRM2 in various aspects of cancer biology, particularly in tumorigenesis and progression [13]. RRM2 promotes the synthesis of deoxyribonucleotides, providing the raw materials required for DNA synthesis, thus facilitating cell division and proliferation [14]. Recent studies have also discovered that RRM2 possesses antioxidant properties, protecting cells from oxidative stress by reducing reactive oxygen species (ROS). This antioxidant effect helps maintain celluar stability and promotes normal cell proliferation [15]. Celastrol may reduce cell proliferation by inhibiting RRM2 expression. Understanding this mechanism is beneficial for elucidating Celastrol's role in tumor therapy and provides new insights for developing novel anti-tumor drugs.

In our study, we aim to explore the mechanism of celastrol in inducing ferroptosis in HCC with the application of bioinformatic analysis, especially network pharmacology, followed by molecular biological experiments including gene expression modulation of RRM2, ferroptosis-related protein expression analysis, and ROS detection. Celastrol is applied to RRM2-modulated HCC cell lines, and changes in the ferroptosis-related phenotypes are to be observed.

In conclusion, our investigation sheds light on the potential therapeutic impact of Cel in liver cancer, emphasizing the induction of ferroptosis as a key mechanism. The identification of RRM2's involvement adds a crucial dimension to this exploration, suggesting its role as a modulator in the observed effects. This study sets the stage for further research, offering a foundation for innovative approaches in liver cancer treatment. The intricate interplay between Cel, ferroptosis, and RRM2 introduces a novel perspective, holding promise for future advancements in precision oncology.

## 2. Materials and Methods

### 2.1. Cell line acquisition and culture

The Huh-7 human HCC cell line (Cell Bank of the Chinese Academy of Sciences, Shanghai, China) was cultured under sterile conditions using Dulbecco's Modified Eagle Medium (DMEM; Hyclone, USA) supplemented with 10 % fetal bovine serum and 1 % penicillin-streptomycin (Gibco, USA). The culture was maintained in a humidified incubator at 37 °C with 5 % CO2. The growth medium was refreshed every 2–3 days, and cells were passaged using trypsin-EDTA solution upon reaching 70–80 % confluence.

### 2.2. Animals and treatment

Animal experiments were approved by the Ethics Committee of Animal Experiments of Shanghai University, China. Balb/c Nude mice were purchased from Charles River (Beijing, China). Animals were housed under 12 h of light and 12 h dark cycle with unrestricted access to food and water unless otherwise described. The mice were adaptively fed for two weeks and randomly assigned to groups of equal size and analysis of all animal samples was carried out in a blinded manner. All animal procedures were approved by the Ethics Committee of Shanghai University on October 18th, 2022 (approval no. 2022-024). All experiments were conducted according to the principles of the Declaration of Helsinki.

For the subcutaneous tumor formation assay, Huh-7 cells ($5 \times 10^6$ cells in 100 μl of PBS) were injected subcutaneously into the nude mice. For Cel experiment, eight-week-old male nude mice were subjected to a 2-week treatment of vehicle or Cel. Inject celastrol into the mice once every two days (celastrol, 1 mg/kg). Cel was dissolved in DMSO and diluted with PBS to a final concentration 1 mg/ml. At the end of the experiment, the mice were anesthetized with pentobarbital sodium before operation and obtained the blood from the abdominal aorta. Serum biochemical indicators are detected by corresponding kit. Some tumor tissue samples were fixed with 4 % paraformaldehyde for subsequent histological examination, and others were stored at −80 °C for subsequent analyses.

### 2.3. CCK-8 cell viability assay

To assess the impact of Cel on Huh-7 cell viability, a Cell Counting Kit-8 (CCK-8, DOJINDO, CK04) assay was performed. $2 \times 10^4$ cells per well were seeded into 96-well plates and allowed to adhere overnight. Subsequently, the culture medium was replaced with fresh DMEM containing various concentrations of Cel ranging from 0 to 8 μM, with or without 5 mM N-acetylcysteine (NAC) (HY–B0215, MedChemExpress, USA) or 100 μM deferoxamine (DFO) (HY–B0988, MedChemExpress, USA). After 24-h incubation of the cells with Cel for 24 h, CCK-8 was added to each well according to the manufacturer's instructions to measure absorbance at 450 nm using a microplate reader (Molecular Devices, USA). The obtained absorbance values were used to calculate the percentage of cell viability and compared with the control group.

### 2.4. Western blot analysis

After Cel treatment, proteins were extracted from both Huh-7 cells and subcutaneous liver cancer tissues of nude mice. The harvested cells and tissues were lysed using RIPA (P0013B, Beyotime, Shanghai, China) buffer containing protease and phosphatase inhibitors. Protein-rich supernatants were obtained by centrifugation, and the protein concentration was determined by bicinchoninic acid assay.

Equal protein amounts were loaded onto SDS-PAGE gels (PG111, Epizyme, China) for separation by electrophoresis, and then transferred to PVDF membranes. The membranes were blocked before incubation with primary antibodies (*p*-mTOR *p*-Ser2481, #6833-1, EPITOMICS; t-mTOR, #6585-1, EPITOMICS; RRM2, #AG3168 Beyotime; xCT, #AF7992, Beyotime; GPX4, #52455, CST; TFR1, #AF8136, Beyotime; β-Actin, #4967, CST) targeting specific ferroptosis-related proteins and internal controls. After washing, the membranes were incubated with the HRP-conjugated secondary antibody (A0239, Beyotime, Shanghai, China). The chemiluminescent signal was visualized using an ECL substrate, and protein bands were captured by a chemiluminescence imaging system (Amersham Imager 600, USA).

### 2.5. Reactive oxygen species (ROS) detection

ROS was measured using a ROS detecting kit (S0033S, Beyotime) according to the manufacturer's instructions. In brief, Huh-7 cells were seeded on glass coverslips after treatment. ROS was visualized using a fluorescent indicator (DCFH-DA), reflecting cellular oxidative stress. Simultaneously, Hoechst stain indicated cell nuclei. Distinct channels for ROS and nuclei were captured by fluorescence microscopy (ZEISS, Axio Observer3).

### 2.6. Malondialdehyde (MDA) assay

Cel-treated Huh-7 cells underwent lysis for cellular component extraction. The MDA level, indicative of lipid peroxidation and oxidative stress, was quantified using an MDA assay kit (S0131S, Beyotime) according to the manufacturer's instructions. After incubation and centrifugation, the absorbance of the sample was measured at 535 nm using a microplate reader (Molecular Devices, USA), and the MDA content was calculated from the standard curve.

### 2.7. Glutathione peroxidase (GSH-Px) activity assay

Reduction in GSH-Px was calculated by detecting its activity using a GSH-Px activity assay kit (S0056, Beyotime) following the manufacturer's instructions, and the recorded activity level was then quantified in milliunits per milligram.

### 2.8. Bioinformatic analysis

#### 2.8.1. Data collection

Microarray data from Gene Expression Omnibus (GEO): Microarray dataset GSE84402 was retrieved from the Gene Expression Omnibus (GEO) database (https://www.ncbi.nlm.nih.gov/geo/). GSE84402 comprises expression data from 28 samples, including 14 tumor tissues and corresponding adjacent tissues obtained from HCC surgical patients.

RNA sequencing data and clinical information from The Cancer Genome Atlas (TCGA): RNA sequencing data and clinical information for HCC were obtained from the liver hepatocellular carcinoma (LIHC) dataset of the TCGA database (https://portal.gdc.cancer.gov/) for further analysis.

Ferroptosis-related genes from FerrDb Database: A set of 484 ferroptosis-related genes was sourced from the FerrDb database (http://www.zhounan.org/ferrdb/current/).

Cel-related targets from Comparative Toxicogenomics Database (CTD): Targets related to Cel were identified through CTD (https://ctdbase.org/).

*2.8.2. Acquisition of differentially expressed genes (DEGs) and construction of protein-to-protein interaction (PPI) network*

The microarray dataset GSE84402 was analyzed using the "limma" package in R software (version 4.3.1) to obtain DEGs. The threshold was set at adj. $P < 0.05$ and $|\log2FC| > 2.5$, resulting in 207 DEGs. Subsequently, the 207 DEGs underwent PPI analysis using the STRING website (https://string-db.org/cgi/). The PPI network was imported into Cytoscape software (version 3.9.1), and the MCODE algorithm was applied to select the most significant clusters, yielding 44 hub genes. Finally, the intersection of hub genes, TCGA prognosis-related genes, ferroptosis-related genes, and celastrol-related targets was performed to obtain the target genes of interest.

*2.8.3. Survival and prognosis analysis*

To determine the survival and prognostic significance of the target genes, relevant data from TCGA-LIHC were obtained. The "survival" package was employed along with Kaplan-Meier curves for OS and progression-free survival (PFS) analyses in HCC patients. Visualization was performed using the "survminer" package.

Receiver operating characteristic (ROC) curves were established using the "timeROC" package to assess the predictive value of the expression level of the target genes for 1-, 3- and 5-year survival periods, using area under the curve (AUC) as the evaluation metric.

Independent factors influencing prognosis were assessed by univariate Cox proportional hazards regression analysis and multivariate Cox proportional hazards regression analysis, and $P < 0.05$ was considered statistically significant. This comprehensive analysis aimed to unveil the survival implications and prognostic values of the identified target genes in HCC patients.

*2.8.4. Gene set enrichment analysis (GSEA)*

The TCGA dataset was stratified into high- and low-expression groups based on the median expression level of the target genes. Enrichment analysis was then conducted using the GSEA software (version 4.3.2), utilizing the HALLMARK database.

*2.8.5. Molecular docking*

The molecular structure of Cel was sourced from the PubChem database (https://pubchem.ncbi.nlm.nih.gov/). Protein structures of the target genes were obtained from the AlphaFold Protein Structure database (https://alphafold.ebi.ac.uk/).

AutoDockTools was employed for the preprocessing of protein receptors and the setup of molecular docking parameters. Molecular docking was executed using AutoDock Vina, and the model with the highest binding affinity was selected from the docking results. Visualization of the molecular docking results was achieved using the Pymol software.

*2.8.6. TCGA analysis of RRM2 in HCC*

RRM2 expression in HCC was examined by using TCGA-LIHC data. The expression level of RRM2 was compared first between HCC and normal liver tissues, and then between paired HCC and adjacent tissues, knowing that these analyses could provide a concise overview about involvement of RRM2 in HCC and highlight potential distinctions in expression patterns.

*2.9. RRM2 overexpression interferes in Huh-7 cells*

RRM2 overexpression in Huh-7 cells was achieved by transfection of cells with the plasmid GV492 (Ubi-MCS-3FLAG-CBh-gcGFP-IRES-puromycin) containing the RRM2 gene. The transfection process was meticulously executed, ensuring precise control and reproducibility of RRM2 overexpression for subsequent experimental analyses.

*2.10. EdU experiment*

For the EdU (5-ethynyl-2′-deoxyuridine) experiment, cells were grouped into four categories: blank, dimethyl sulfoxide (DMSO), 3 μM Cel treatment, and RRM2 overexpression. The incorporation of EdU into replicating DNA allowed for the assessment of cell proliferation dynamics in each group. After incubation, samples were observed under a fluorescence microscope (Axio Observer3, ZEISS). The distinct groups were carefully defined to capture the specific effects of Cel and RRM2 overexpression, ensuring a comprehensive analysis of their impact on cell proliferation.

*2.11. Wound healing experiment*

Huh-7 cells in the monolayer were intentionally scratched, and the subsequent migration of cells into the wounded area was measured and observed at 0 and 24 h. This assay aimed to evaluate the impact of 3 μM Cel treatment and RRM2 overexpression on cell migration dynamics.

*2.12. Transwell experiment for migration and invasion*

The Transwell experiment included migration and invasion assays. Cells were seeded at a density of $1 \times 10^4$ cells per well and then subjected to experimental conditions such as 3 μM Cel treatment and RRM2 overexpression. The assay was conducted over 72 h. In the

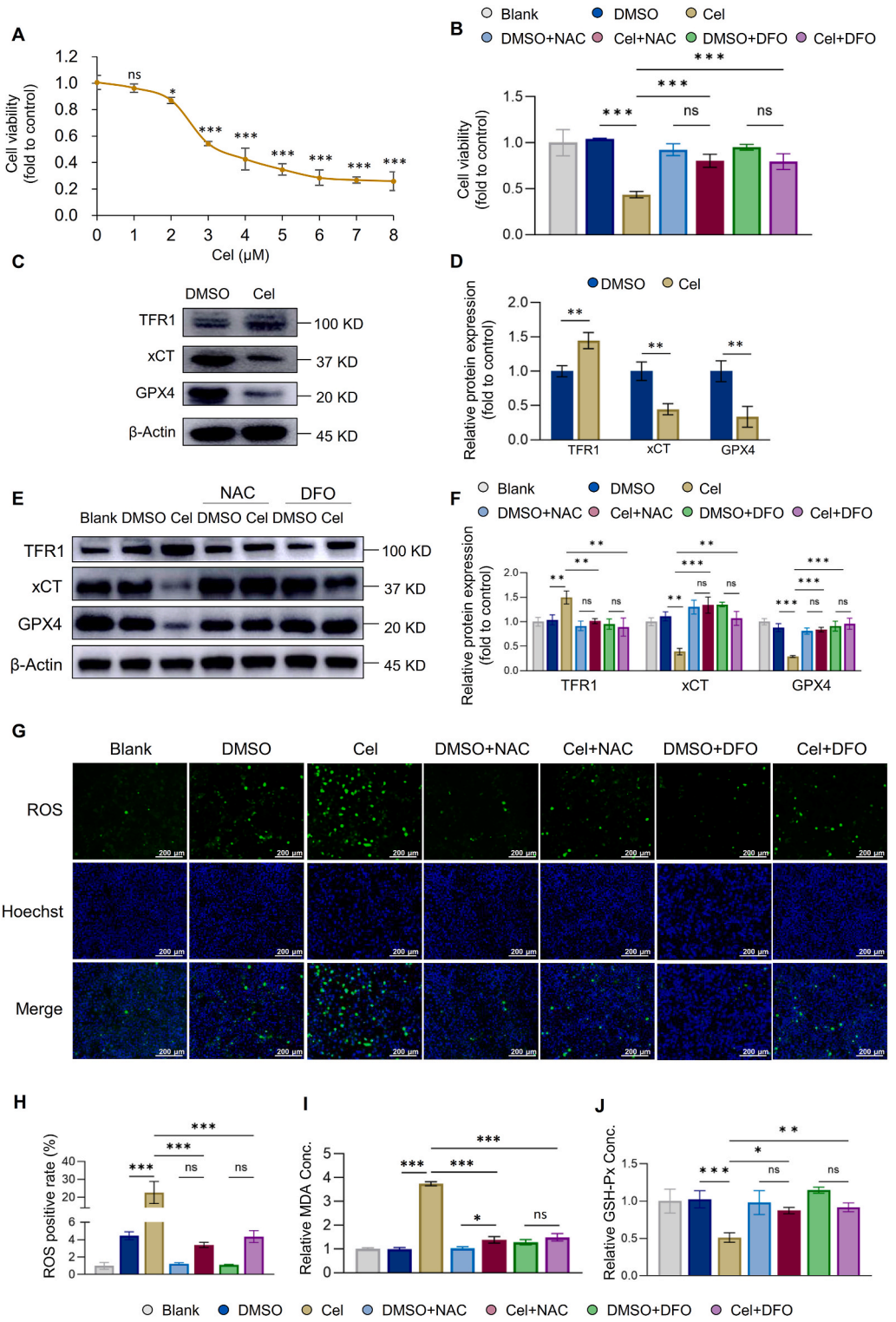


**Fig. 1.** Effects of celastrol (Cel) on cytotoxicity, ferroptosis, and TFR1-xCT-GPX4 pathway modulation in Huh-7 Cells. **A**: Cel induced dose-dependent cytotoxicity in Huh-7 cells. Cell viability was assessed by CCK-8 assay after 24-h treatment with varying concentrations (0–8 μM) of Cel. **B**: CCK-8 cell viability assay revealing the inhibition of 3 μM Cel-induced cell death by ferroptosis antagonists. 5 mM N-acetylcysteine (NAC) and 100 μM deferoxamine (DFO) were introduced to Cel-treated cells, revealing a mitigating effect on Cel-induced cytotoxicity. **C, D**: Representative Western blot images and bar chart demonstrating the modulation of Cel on the expression of proteins in TFR1-xCT-GPX4 ferroptotic pathway. TFR1 expression was upregulated, while xCT and GPX4 expressions were downregulated following Cel treatment. **E, F**: Representative Western blot

images and bar chart demonstrating the antagonism of Cel-induced effects by ferroptosis inhibitors. The addition of NAC and DFO during Cel treatment counteracted the alterations in TFR1, xCT, and GPX4 expressions. **G, H**: Representative ROS images and bar chart demonstrating the antagonism of Cel-induced effects by ferroptosis inhibitors. **I**: MDA detection. **J**: GSH-Px detection. *p*-values were determined by one-way ANOVA. $^{*}P < 0.05$, $^{**}P < 0.01$, $^{***}P < 0.001$. All data are representative of three independent experiments, and the values are expressed as the mean ± SD.

invasion assay, cells were seeded onto Transwell inserts coated with a Matrigel (356234, Corning, USA) barrier. The invasive potential of cells and the migrated cells was evaluated over 72 h.

### 2.13. Biochemical analysis of blood samples

Using commercial assay kits, blood samples from the athymic nude mice were analyzed for biochemical indicators including the aspartate aminotransferase (AST), alanine aminotransferase (ALT), creatinine (Cr), uric acid (UA), total bilirubin (T-BIL), and lactate dehydrogenase (LDH).

### 2.14. Immunohistochemistry (IHC) staining

IHC staining was performed to investigate the expression of RRM2 in the tumor samples. Representative images were captured at 10 × and 40 × magnifications, corresponding to specific fields. Hematoxylin and eosin (HE) staining was concurrently conducted to provide context to cellular morphology.

### 2.15. ChatGPT 3.5 refinement

The manuscript underwent language refinement using ChatGPT 3.5 for improved clarity and academic adherence. The authors guided the process with specific instructions.

### 2.16. Statistical analysis

Statistical analysis was conducted using SPSS version 19.0 (IBM Corp., Armonk, NY, USA). Results were expressed as the means ± standard deviations of 3 or more independent experiments. Student's t-test was used for comparisons of two groups. One-way or two-way ANOVA, followed by Tukey's post hoc test, was used for comparisons of three or more groups. Values were considered significantly different if the *P*-value was less than 0.05.

## 3. Results

### 3.1. Cel induces ferroptosis in HCC cell lines

To address the impact of Cel on liver cancer cell viability, we first performed CCK-8 assay to investigate the cytotoxic effect of Cel on Huh-7 cells by exposing cells to varying concentrations (0–8 μM) of Cel for 24 h. As depicted in Fig. 1A, the results showed that celastrol causes Huh-7 cell death in a dose-dependent manner. The half-maximal inhibitory concentration (IC50) of celastrol treatment for 24 h was calculated to be 3 μmol/L.

Based on the aforementioned findings, we further investigated whether 3 μM Cel-induced cell death in liver cancer cells was mediated through the induction of ferroptosis. We introduced the ferroptosis antagonist N-acetylcysteine (NAC) or deferoxamine (DFO) to Cel-treated cells. The result of CCK-8 assay showed that both antagonists inhibited the Cel-induced cell death in liver cancer cells (Fig. 1B).

To further substantiate that Cel induced ferroptosis in liver cancer cells, we employed Western blot experiments to validate this effect at the protein level. Along the ferroptotic pathway involving TFR1-xCT-GPX4, 3 μM Cel was found to enhance the expression of TFR1 and suppress the expression of xCT and GPX4 (Fig. 1C, D). Additionally, the concurrent addition of the ferroptosis inhibitors NAC and DFO during Cel treatment antagonized the aforementioned effect (Fig. 1E, F).

The generation of ROS is a crucial indicator of cellular ferroptosis. Through immunofluorescence experiments, we observed that Cel treatment increased ROS production in Huh-7 cells. Concurrent administration of the ferroptosis inhibitor NAC or DFO antagonized this effect induced by Cel (Fig. 1G, H).

Similarly, the production of MDA and the consumption of GSH-Px are indicative of ferroptosis. Therefore, using MDA and GSH detection kits, we assessed the concentrations of these substances in liver cancer cells treated with Cel. The results showed that the MDA level was increased while the GSH level was decreased in Huh-7 cells after Cel treatment. When Cel was co-administered with NAC or DFO, this effect of Cel was mitigated (Fig. 1I, J).

### 3.2. RRM2 is a crucial gene in Cel-induced ferroptosis in liver cancer cells

To unravel the specific mechanism underlying Cel-induced ferroptosis in liver cancer, we conducted bioinformatics analysis using online databases. Initially, we retrieved liver cancer-associated DEGs from the HCC dataset (GSE84402) in the TCGA database

(Fig. 2A). Subsequently, we subjected the identified 207 DEGs to PPI analysis using the STRING database (https://string-db.org/cgi/) (Fig. 2B). The resultant PPI network was imported into Cytoscape software (version 3.9.1), and the MCODE algorithm was employed to identify the most significant cluster, yielding 44 candidate genes (Fig. 2C).

Conclusively, a Venn diagram was constructed incorporating the 44 candidate genes, 3006 genes associated with liver cancer prognosis from TCGA, 484 Ferroptosis-related genes, and 209 Celtargets. This analysis unveiled the target genes of interest, notably highlighting RRM2 (Fig. 2D).

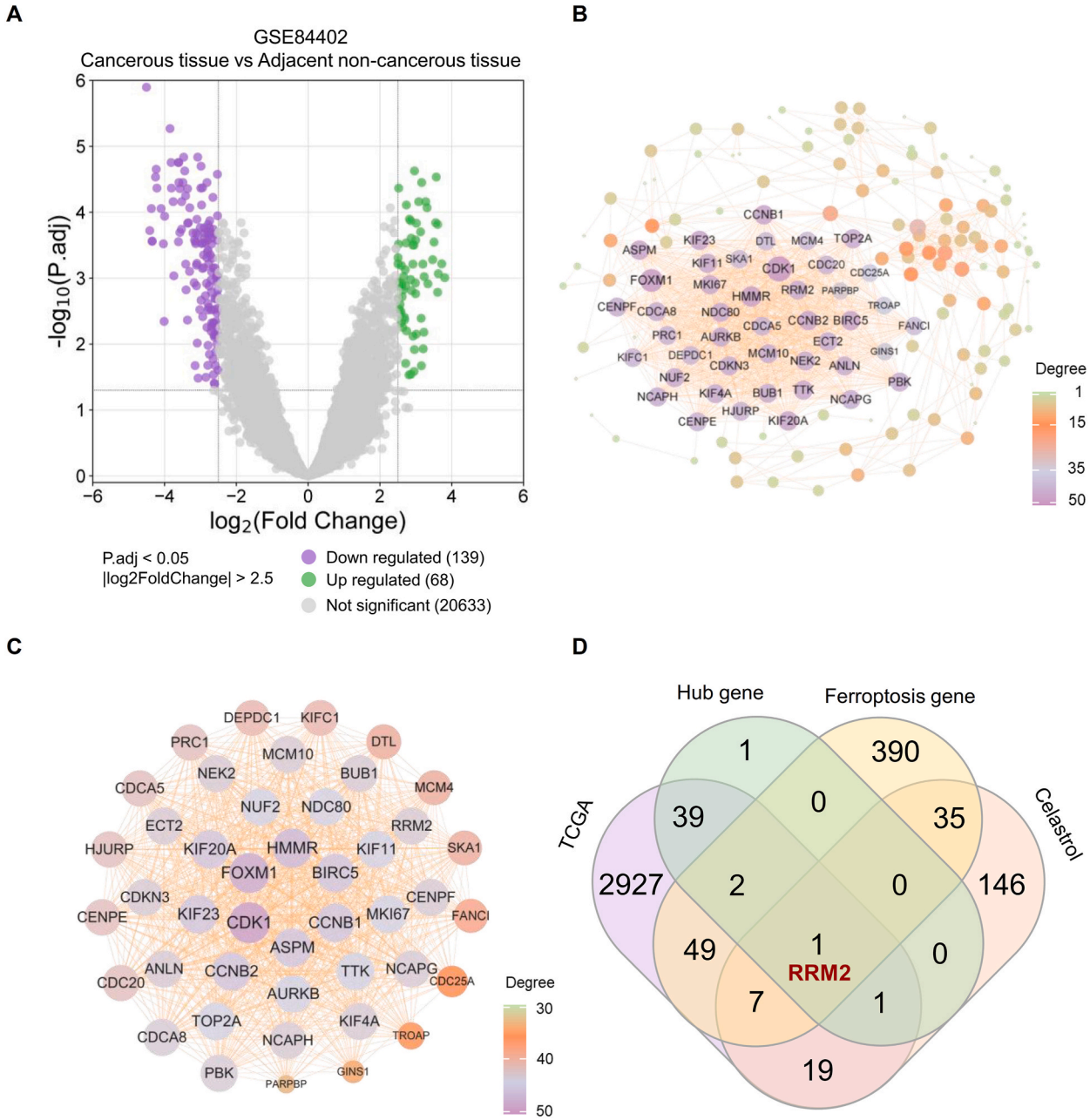


**Fig. 2.** Integrated analysis of liver cancer-associated differentially expressed genes (DEGs) and identification of RRM2 as a target gene. **A**: Identification of liver cancer-associated differentially expressed genes (DEGs) from the TCGA-LIHC dataset. The threshold was set at adj. $P < 0.05$ and $|\log2FC| > 2.5$, resulting in 207 DEGs. **B**: Protein-protein interaction (PPI) analysis of the 207 identified DEGs using the STRING database. The purple color represents a stronger connection, and the green color stands for a weaker one. **C**: Selection of the most significant cluster in the above PPI network using the MCODE algorithm, resulting in 44 hub genes. **D**: Venn diagram illustrating the intersection of the 44 hub genes, 3006 genes associated with liver cancer prognosis (TCGA), 484 Ferroptosis-related genes, and 209 Cel targets, highlighting RRM2 as the target gene of interest.

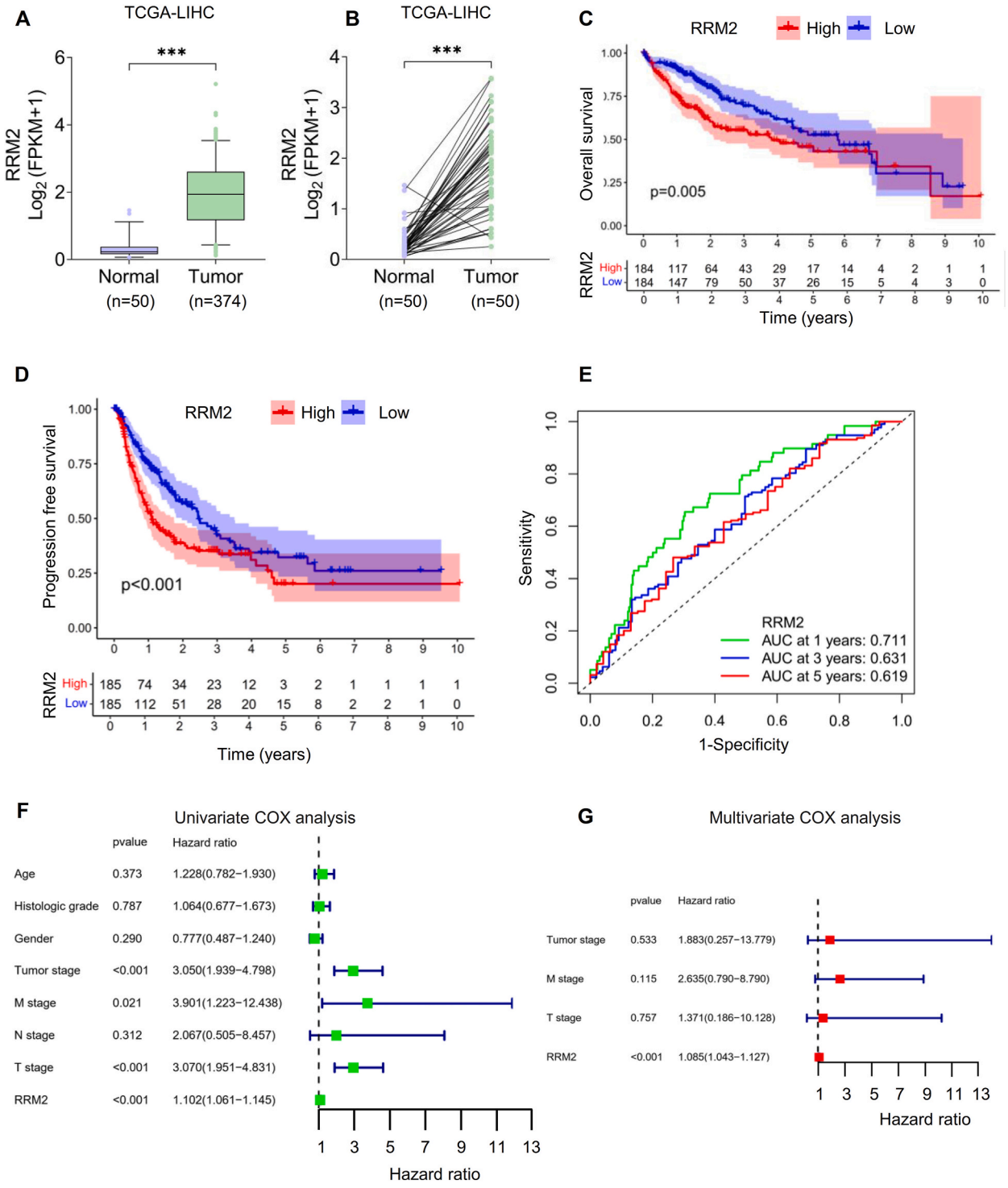


**Fig. 3.** RRM2 expression is negatively correlated with the prognosis of liver cancer. **A**: Upregulation of RRM2 expression in liver cancer tissues (n = 374) compared to normal liver tissues (n = 50) in TCGA-LIHC dataset. **B**: Elevated expression of RRM2 in liver cancer tissues compared to paired adjacent non-cancerous tissues (n = 50). **C, D**: Survival analysis of TCGA-LIHC dataset indicating lower overall survival (OS) and progression-free survival (PFS) in patients with higher RRM2 expression. **E**: Receiver Operating Characteristic (ROC) curves demonstrating the predictive capability of RRM2 expression for the survival outcomes of liver cancer patients at 1, 3, and 5 years. **F**: Univariate Cox proportional hazards regression analysis highlighting RRM2 expression as a prognostic risk factor. **G**: Multivariate Cox proportional hazards regression analysis confirming RRM2 expression as an independent prognostic risk factor.

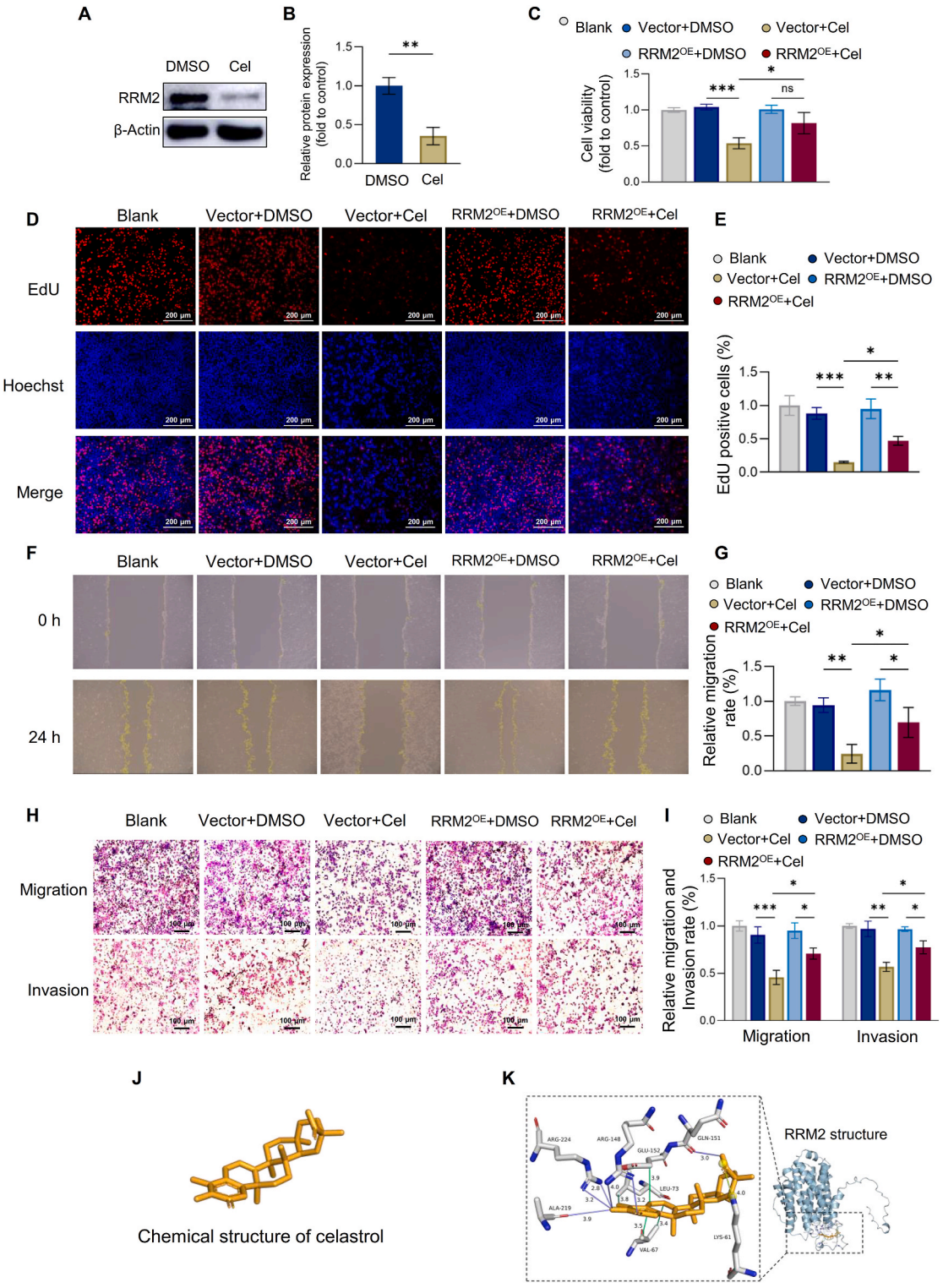


**Fig. 4.** Experimental validation, functional analysis and molecular simulation of celastrol (Cel) and RRM2 in liver cancer cells. **A, B**: Western blot analysis showing the significant inhibition of RRM2 protein expression in Huh-7 cells treated with Cel for 24 h. **C**: CCK-8 cell viability assay indicated that RRM2 overexpression attenuated the cytotoxic effects of Cel on liver cancer cells. "OE" stands for overexpression. **D, E**: EdU assay demonstrated that RRM2 overexpression counteracted the proliferation inhibitory effect of Cel on Huh-7 cells. **F–I**: Wound healing (F, G), transwell migration and invasion assays (H), and their statistical bar charts (I) revealed that RRM2 overexpression partially antagonized the inhibitory effects of Cel on the malignant behavior of liver cancer cells. **J, K**: Molecular simulation and molecular docking simulation of Cel with RRM2 using

AutoDock Vina. The green lines represent hydrophobic interactions, the blue lines represent hydrogen bonds, and the yellow lines represent salt bridges. The scale is as shown in the representative images. *p*-values were determined by one-way ANOVA. $^{*}P < 0.05$, $^{**}P < 0.01$, $^{***}P < 0.001$. All data are representative of three independent experiments, and the values are expressed as the mean ± SD.

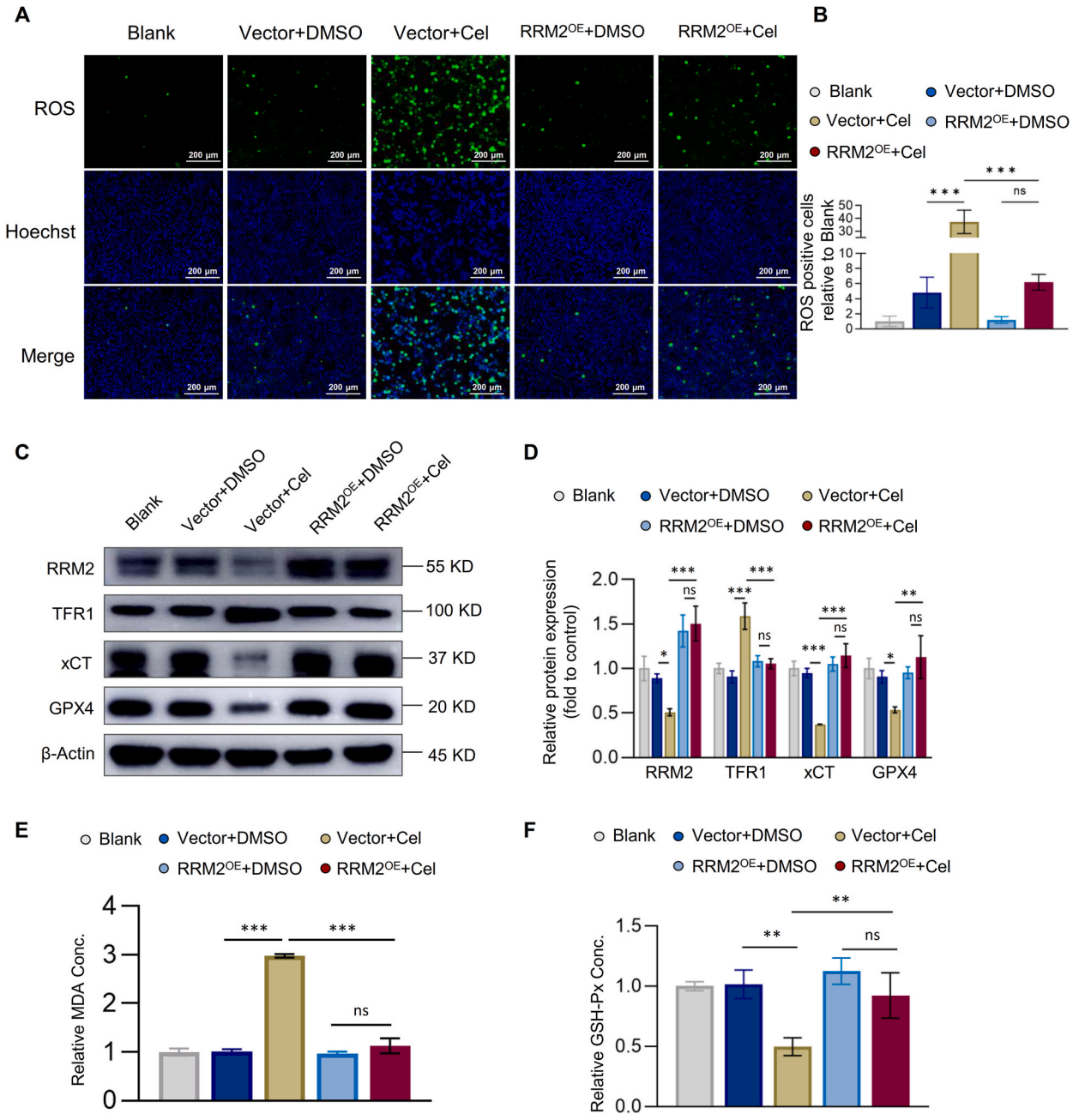


**Fig. 5.** Overexpression of RRM2 inhibits the activation of the ferroptosis pathway in Huh-7. **A, B**: Representative images of immunofluorescence ROS assay showing increased tolerance to Cel (3 μM) Huh-7 cells overexpressing RRM2, with significantly lower ROS production compared to the control group. The scale is as shown in the images. **C, D**: Western blot analysis and its statistical bar chat indicated that RRM2 overexpression inhibited the activation of the ferroptosis pathway (representative protein expression of TFR1, xCT, and GPX4) in liver cancer cells induced by Cel. **E, F**: Detection of MDA and GSH-Px levels in cells showed that overexpression of RRM2 suppressed the Cel-induced increase in MDA and decrease in GSH-Px. *p*-values were determined by one-way ANOVA. $^{*}P < 0.05$, $^{**}P < 0.01$, $^{***}P < 0.001$. All data are representative of three independent experiments, and the values are expressed as the mean ± SD.

### 3.3. RRM2 expression is negatively correlated with the prognosis of liver cancer

To investigate the clinical relevance of RRM2 in liver cancer, we conducted bioinformatic analysis on the TCGA-LIHC dataset. As shown in Fig. 3A, the RRM2 expression was significantly upregulated in the liver cancer tissue compared with that in the normal liver tissue. Additionally, the RRM2 expression in the liver cancer tissue was significantly elevated as compared with that in the paired adjacent non-cancerous tissue (Fig. 3B).

Survival analysis of patients from the HCC dataset revealed that both OS and PFS were lower in individuals with higher RRM2 expression levels (Fig. 3 C, D).

ROC curves further illustrated the robust predictive capability of RRM2 expression for the survival outcomes of liver cancer patients, with AUC values of 0.711, 0.631 and 0.619 at 1, 3 and 5 years, respectively (Fig. 3E).

Independent factors impacting the prognosis of HCC patients were shown by univariate Cox proportional hazards regression analysis (Fig. 3F) and multivariate Cox proportional hazards regression analysis (Fig. 3G). The models consistently identified RRM2 expression as an independent prognostic risk factor in both univariate and multivariate analyses.

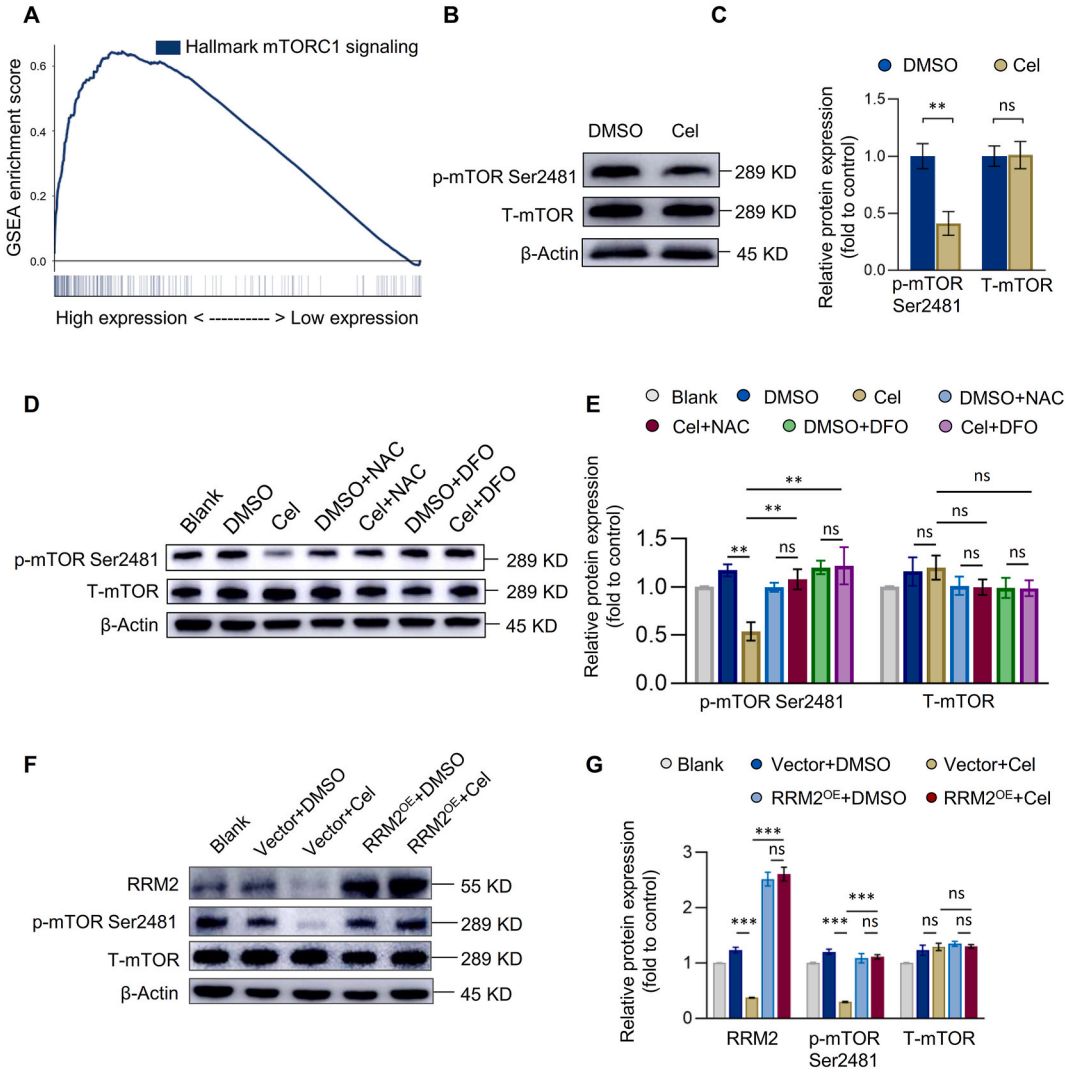


**Fig. 6.** Celastrol inhibits mTOR phosphorylation through RRM2. **A**: GSEA analysis revealing upregulation enrichment of the mTOR pathway represented by the gene set "HALLMARK_MTORC1_SIGNALING" in HCC samples. **B, C**: Western blot results and their statistical bar chart showed that Cel (3 μM) inhibited mTOR phosphorylation in Huh-7 cells. **D, E**: Western blot results and their statistical bar chart indicating ferroptosis inhibitors 5 mM NAC and 100 μM DFO counteracting the promoting effect of Cel (3 μM) on mTOR phosphorylation. **F, G**: Western blot and its statistical bar chart showed that in Huh-7 cells overexpressing RRM2, and the inhibitory effect of Cel (3 μM) on mTOR phosphorylation was significantly attenuated. *p*-values were determined by one-way ANOVA. $^{*}P < 0.05$, $^{**}P < 0.01$, $^{***}P < 0.001$. All data are representative of three independent experiments, and the values are expressed as the mean ± SD.

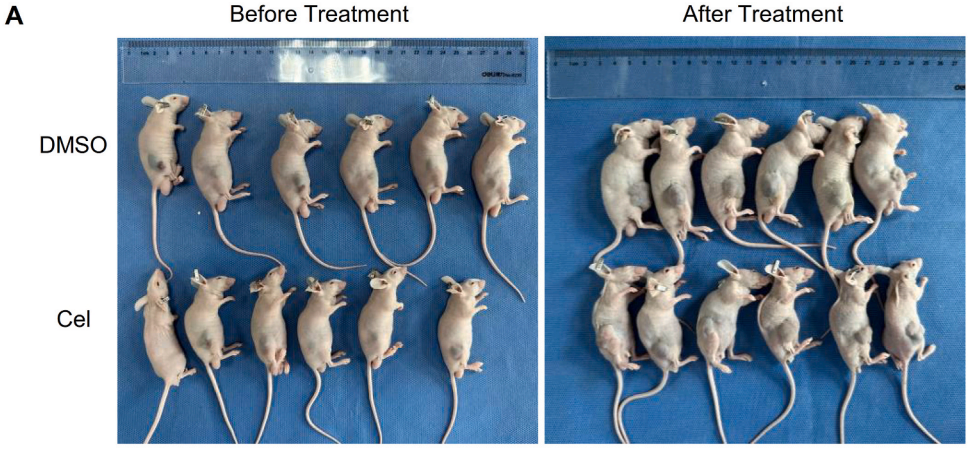


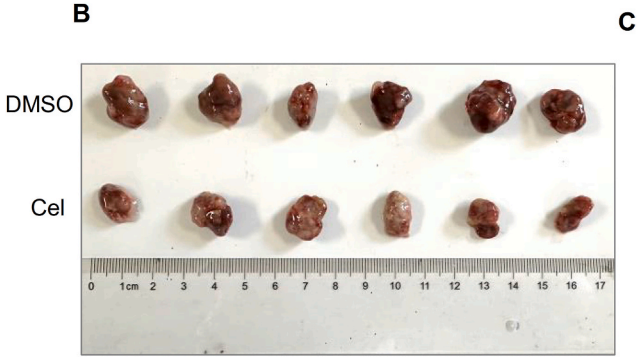


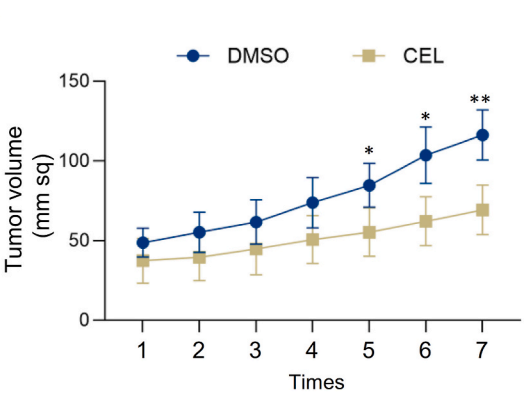


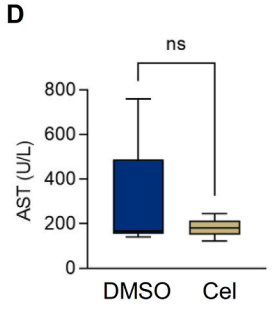


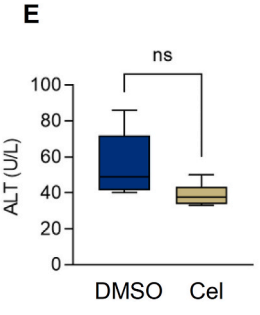


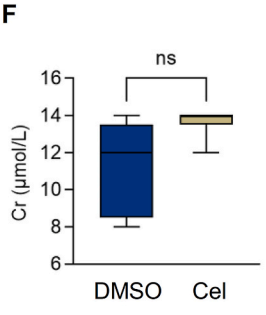


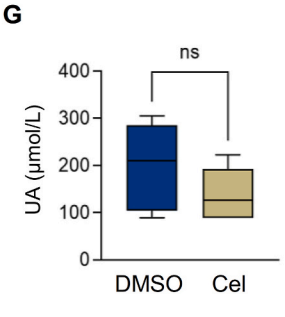


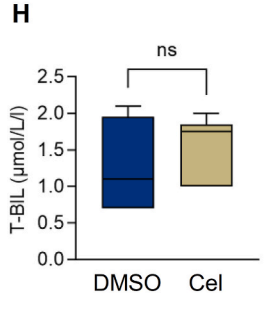


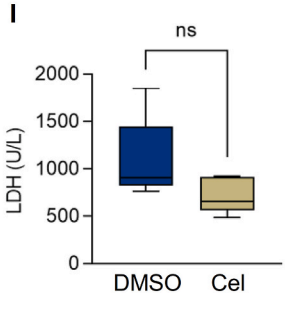


(caption on next page)

**Fig. 7.** Celastrol (Cel) shows showed promising therapeutic efficacy and safety in mouse xenograft models. **A, B**: Tumor volume in Cel (1 mg/kg) treatment group (n = 6) was smaller than that in the control group (n = 6) in the subcutaneous xenograft experiment in nude mice. Two groups received normal diet for 14 days; each group was then given Cel or DMSO for 14 days. The tumor size is as shown in figure. **C**: Growth curves demonstrated that the growth rate of tumors in Cel treatment group was slowed down. "mm sq" stands for "square millimeters". **D-I**: Blood sample analysis revealing no significant impact of Cel treatment on AST (D), ALT (E), Cr (F), UA (G), T-BIL (H), and LDH (I) concentrations in mouse blood. *p*-values were determined by one-way ANOVA. $*P < 0.05$, $**P < 0.01$, $***P < 0.001$. All data are representative of three independent experiments, and the values are expressed as the mean ± SD.

### 3.4. Celastrol anti-tumor effects can be antagonized by the overexpression of RRM2 and might bind to the RRM2 protein

Based on the aforementioned bioinformatic analysis results, we will verify the effect of Celastrol on RRM2 expression. Using Western blot experiments, we found that treatment with 3 μM Celastrol for 24 h significantly inhibited the expression of RRM2 in Huh-7 cells (Fig. 4A, B). To investigate whether Celastrol regulates the malignant phenotype of liver cancer through RRM2, we used lentiviral vectors to induce overexpression of RRM2 in Huh-7 cells. The CCK-8 cell viability assay revealed that overexpression of RRM2 diminishes the inhibitory effect of Celastrol on cell proliferation (Fig. 4C). EdU assays indicated that RRM2 overexpression counteracted the inhibitory effect of Cel on Huh-7 cell proliferation (Fig. 4D, E). In addition, wound healing, transwell migration and invasion assays revealed that Cel inhibited the migration and invasion capabilities of liver cancer cells, while RRM2 overexpression partially antagonized the inhibitory effect of Cel on the malignant behavior of liver cancer cells (Fig. 4F–I).

To further understand how Celastrol inhibits RRM2 expression, we conducted molecular docking experiments between Celastrol and RRM2. The analysis revealed that Celastrol forms four hydrophobic interactions, six hydrogen bonds, and one salt bridge with RRM2. Hydrophobic interactions and hydrogen bonds typically do not lead to protein degradation, while compound-protein salt bridges can inhibit protein activity, resulting in protein degradation. Celastrol forms a salt bridge with LYS-61A of RRM2, which may be one of the mechanisms by which Celastrol reduces RRM2 expression (Fig. 4J, K).

### 3.5. RRM2 overexpression inhibits Cel-induced ferroptosis

The preceding experiments provided initial insights into the inhibitory role of RRM2 in the pharmacological effects of Cel. To further investigate whether RRM2 interfered with Cel-induced ferroptosis in liver cancer cells, we treated both wild-type Huh-7 cells and Huh-7 cells overexpressing RRM2 with Cel for 24 h, and then observed ROS generation through immunofluorescence assays. The results showed that Huh-7 cells overexpressing RRM2 exhibited the increased tolerance to Cel stimulation, as represented by a significant reduction in ROS production compared with the control group (Fig. 5A, B).

Next, we conducted a Western blot experiment to examine the expression changes of key proteins (TFR1, xCT and GPX4) in the ferroptosis pathway in the aforementioned normal Huh-7 cells and RRM2-overexpressing Huh-7 cells. The results demonstrated that RRM2 overexpression inhibited the activation of the ferroptosis pathway in liver cancer cells induced by Cel (Fig. 5C, D). Similarly, using assay kits, we detected MDA and GSH-Px levels in cells from the mentioned groups. RRM2 overexpression was found to suppress the Cel-induced increase in MDA and decrease in GSH-Px (Fig. 5E, F).

### 3.6. Celastrol inhibits mTOR phosphorylation through RRM2

To investigate how RRM2 affected Cel-induced ferroptosis in liver cancer cells, we conducted GSEA on gene expression data from HCC patients. The result demonstrated significant upregulation enrichment of the mTOR pathway as represented by the gene set "HALLMARK_MTORC1_SIGNALING," with an enrichment score of 0.65 and a *p*-value of 0.001 (Fig. 6A). This suggests that in HCC samples, the gene set associated with the mTOR signaling pathway was significantly upregulated.

mTOR, as a key regulator of cellular metabolism, may impact iron uptake and utilization by influencing various cellular signaling pathways. Components like mTORC1 have been found to interact with iron-regulating proteins, potentially influencing cellular sensitivity to iron and OS [16]. Western blot results indicated that Cel inhibited the phosphorylation of mTOR in Huh-7 cells (Fig. 6B, C). Notably, the ferroptosis inhibitors NAC and DFO counteracted the promoting effect of Cel on these phosphorylation events (Fig. 6D, E).

Interestingly, in Huh-7 cells overexpressing RRM2, the inhibitory effect of Cel on mTOR phosphorylation was significantly attenuated (Fig. 6F, G), suggesting that RRM2 may play a potential regulatory role in modulating the impact of Cel on the mTOR signaling pathway in liver cancer cells.

### 3.7. In vivo therapeutic efficacy of Cel on HCC

To further investigate the therapeutic effect of Cel on liver cancer in a live environment, we conducted a subcutaneous xenograft experiment in nude mice by injecting $1 \times 10^5$ liver cancer cells mixed with matrigel into the right dorsal side of the nude mice to establish a subcutaneous tumor model. After 2-week implantation, the experimental group (n = 6) and the control group (n = 6) were treated with Cel of 1 mg/kg or DMSO, respectively, for 7 times. We monitored tumor growth, collected blood samples, and harvested subcutaneous tumor tissues at the end of the 14-days treatment period. The mice were then euthanized using cervical dislocation.

The results demonstrated that the tumor volume in the Cel treatment group was smaller than that in the control group (Fig. 7A, B), with a relatively slower growth rate (Fig. 7C). Blood sample analysis revealed no significant impact of Cel treatment on AST, ALT, Cr,

UA, T-BIL, and LDH concentrations in mouse blood (Fig. 7D–I), indicating that Cel was safe in clinical application.

Further analysis of tumor tissues from 12 nude mice by Western blotting showed that Cel treatment inhibited the expression of RRM2 in tumors, activated the TFR1/xCT/GPX4 ferroptosis pathway, and concurrently suppressed the phosphorylation of mTOR (Fig. 8A, B). IHC staining of subcutaneous tumor tissues confirmed the inhibitory effect of Cel on RRM2 in tumor tissues (Fig. 8C, D). Additionally, the MDA concentration in the Cel treatment group was significantly higher than that in the control group (Fig. 8E), and the GSH-Px concentration was lower in tumor tissues (Fig. 8F).

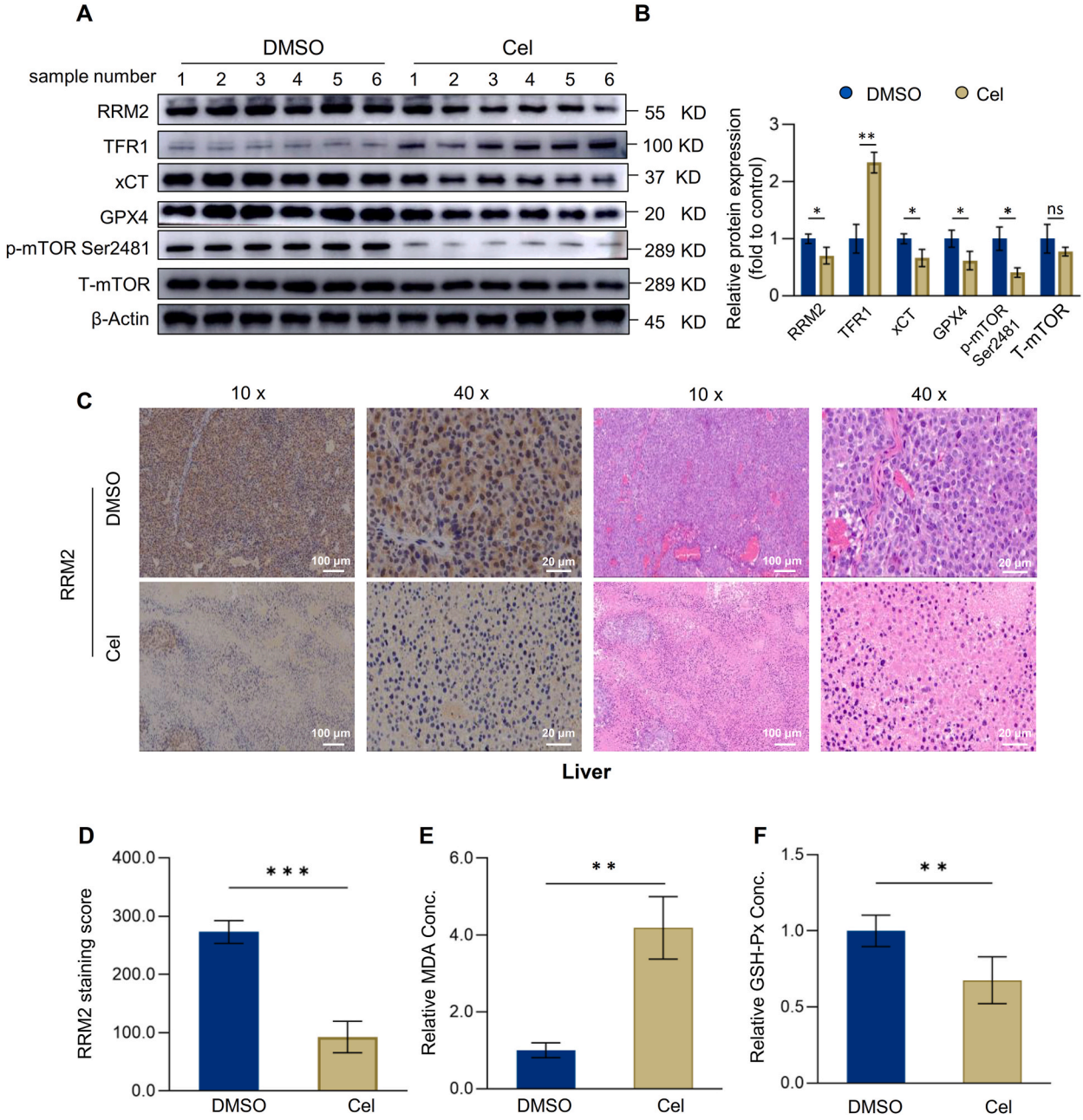


**Fig. 8.** Ferroptosis pathway in mouse xenograft tissues was inhibited by celastrol (Cel) **A, B**: Western blot results and their statistical bar chart showed that Cel inhibited RRM2 expression, activation of the TFR1/xCT/GPX4 ferroptosis pathway, and suppression of mTOR phosphorylation in subcutaneous tumor tissues. **C, D**: Immunohistochemistry staining confirmed the inhibitory effect of Cel on RRM2 in tumor tissues. The scale and magnification rates are as shown in the representative images. **E**: The MDA concentration in tumor tissues of Cel treatment group was higher than that of the control group. **F**: The GSH-Px concentration in tumor tissues of Cel treatment group was lower than that of the control group. *p*-values were determined by one-way ANOVA. $^{*}P < 0.05$, $^{**}P < 0.01$, $^{***}P < 0.001$. All data are representative of three independent experiments, and the values are expressed as the mean ± SD.

## 4. Discussion

Ferroptosis is a novel type of programmed cell death characterized by iron-dependent lipid peroxidation, distinguishing it from traditional apoptosis and necrosis [17,18]. Tumor cells, with their higher metabolic rates and oxidative stress levels, are more susceptible to ferroptosis [19]. This process induces lipid peroxidation in tumor cells by increasing intracellular iron ion and reactive oxygen species (ROS) levels, leading to cell membrane rupture and subsequent cell death. In contrast, normal cells exhibit lower sensitivity to ferroptosis, presenting an opportunity to selectively target tumor cells. Celastrol exhibits significant anti-tumor effects through various mechanisms. It primarily inhibits tumors by inducing apoptosis, suppressing the NF-κB pathway, generating ROS, and inhibiting the PI3K/mTOR pathway [20–22].

Recent studies have shown that Celastrol can induce ferroptosis. Celastrol, a novel inducer of ferroptosis, significantly alters cellular iron metabolism, resulting in elevated iron ion levels. These excess iron catalyze the Fenton reaction, producing a substantial amount of ROS [23]. The accumulation of ROS triggers lipid peroxidation, disrupting membrane structure and ultimately causing cell death. Emerging evidence indicated that ferroptosis plays an important role in tumor therapy. Recent research reported that Cel confers ferroptosis resistance via AKT/GSK3β signaling in high-fat diet-induced cardiac injury [23]. Celastrol is also reported to induce ferroptosis in activated hepatic stellate cells to ameliorate hepatic fibrosis via targeting peroxiredoxins and heme oxygenase 1 [9]. In the field of oncology, researchers also find ferroptosis crucial. Ferroptosis inducer erastin sensitizes non-small cell lung cancer cells to celastrol through activation of the ROS-mitochondrial fission-mitophagy axis [9]. The detailed mechanism of celastrol's effect on certain biological processes remained uncertain.

RRM2, also known as ribonucleotide reductase small subunit 2, serves as a crucial player in tumorigenesis and developmental processes. As an integral component of nucleotide reductase, RRM2 holds significant sway over DNA synthesis and repair mechanisms [24]. It accelerates DNA synthesis, furnishing the necessary building blocks for tumor cell proliferation. Moreover, during instances of DNA damage and stress, RRM2 steps in to aid DNA repair by supplying deoxyribonucleotide triphosphates (dNTPs) [12]. Notably, research highlights RRM2's heightened expression in tissues afflicted with Sunitinib-resistant renal cell carcinoma and renal carcinoma, where it further exacerbates resistance to Sunitinib by activating the AKT pathway [25]. Furthermore, investigations have underscored the upregulation of RRM2 in breast and lung cancers [26]. Given its implicated role in tumorigenesis, RRM2 emerges as a prime target for anti-tumor interventions. Inhibitors designed to target RRM2 hold promise in impeding tumor cell proliferation and augmenting tumor susceptibility to chemotherapy and radiotherapy, thereby fostering improved treatment outcomes.

In this study, we employed modern medical research methods such as bioinformatics analysis, cell biology experiments, molecular biology experiments, and animal experiments to elucidate the potential action mechanism of Cel (an active component of the traditional Chinese medicine) by inducing ferroptosis in liver cancer cells via inhibition of the crucial gene RRM2. Our cell experiments confirmed the anti-tumor effect of Cel on liver cancer cells, and our bioinformatics analysis also revealed the interaction between Cel and RRM2 and its association with the mTOR signaling pathway. Our further cell experiments demonstrated the inhibitory effect of Cel on RRM2 expression in Huh-7 cells by activating the ferroptosis signaling pathway (TFR1/xCT/GPX4).

While previous studies addressed the role of Cel in cancer treatment [27,28], our study further confirmed its safety, showing no impairment to the liver/kidney function in mice receiving Cel treatment. Our bioinformatics analysis identified ferroptosis as a potential mechanism underlying the anticancer effect of Cel. Additionally, the discovery and validation of RRM2 as a key gene provide potential molecular targets and prognostic markers for liver cancer drug treatment.

However, limitations of the present research cannot be ignored. Our study can benefit from real-world results of Cel application in liver cancer patients, providing more comprehensive insights into its effectiveness and safety in clinical practice. Additionally, while our reliance on public databases has limitations, the wealth of data accessed enhances the generalizability of our findings. Moreover, further exploration and validation on the detailed mechanism of how Cel promoted RRM2 degradation are needed in the future study.

## 5. Conclusion

In this study discovers and validates the phenomenon and mechanism of Cel inducing ferroptosis in liver cancer through RRM2, providing new potential targets and treatment strategies for liver cancer drug therapy.

## Data availability statement

The TCGA and GEO data used in this study are available in public databases (relevant web pages are provided in the article). The raw data from the Western blot experiments has been stored in the GitHub database and can be accessed publicly at https://github.com/NNYY0606/Raw-data/blob/main/supplementary%20material.pdf. Experiments data from this study can be obtained by contacting the corresponding author.

## Ethics statement

All animal procedures were approved by the Ethics Committee of Shanghai University on October 18th, 2022 (approval no. 2022-024). All experiments were conducted according to the principles of the Declaration of Helsinki.

## Consent for publication

All the authors have provided consent for the publication.

## Funding

This work was supported by Research Grant for Health Science and Technology of Pudong Health Bureau of Shanghai (Grant No. PW2023A-19) and Young Medical Talents Training Program of Pudong Health Bureau of Shanghai (Grant No. PWRq2020-61). Shanghai Municipal Health Commission Research Project (201840082, 202040068).

## CRediT authorship contribution statement

**Xue Zhang:** Writing – original draft, Project administration, Methodology, Investigation. **Manman Qi:** Methodology, Investigation. **Kailun Huo:** Software, Project administration, Conceptualization. **Banglan Cai:** Software. **Jian Zhang:** Software. **Yijun Tian:** Writing – original draft, Project administration. **Denghai Zhang:** Writing – original draft, Project administration.

## Declaration of competing interest

The authors declare that they have no known competing financial interests or personal relationships that could have appeared to influence the work reported in this paper.

## Appendix A. Supplementary data

Supplementary data to this article can be found online at https://doi.org/10.1016/j.heliyon.2024.e33936.

## References

[1] A. Vogel, T. Meyer, G. Sapisochin, R. Salem, A. Saborowski, Hepatocellular carcinoma, Lancet 400 (2022) 1345–1362, https://doi.org/10.1016/s0140-6736(22)01200-4.
[2] Y.N. Avtaeva, I.S. Mel'nikov, O.S. Saburova, K.G. Guriya, M.C. Osidak, C.P. Domogatsky, Z.A. Gabbasov, Complex Interaction of Platelets, von Willebrand Factor and Leukocytes, in Whole Blood at High Shear Rates Is Mediated by Platelet GPIIb/IIIa Receptor, Bull. Exp. Biol. Med. 171 (2021) 588–591, https://doi.org/10.1007/s10517-021-05274-5.
[3] Z.J. Brown, D.I. Tsilimigras, S.M. Ruff, A. Mohseni, I.R. Kamel, J.M. Cloyd, T.M. Pawlik, Management of hepatocellular carcinoma: a review, JAMA Surg 158 (2023) 410–420, https://doi.org/10.1001/jamasurg.2022.7989.
[4] C. Yang, H. Zhang, L. Zhang, A.X. Zhu, R. Bernards, W. Qin, C. Wang, Evolving therapeutic landscape of advanced hepatocellular carcinoma, Nat. Rev. Gastroenterol. Hepatol. 20 (2023) 203–222, https://doi.org/10.1038/s41575-022-00704-9.
[5] A. Fernández, R. Ordóñez, R.J. Reiter, J. González-Gallego, J.L. Mauriz, Melatonin and endoplasmic reticulum stress: relation to autophagy and apoptosis, J. Pineal Res. 59 (2015) 292–307, https://doi.org/10.1111/jpi.12264.
[6] G. Majno, I. Joris, Apoptosis, oncosis, and necrosis. An overview of cell death, Am. J. Pathol. 146 (1995) 3–15.
[7] G. Lei, L. Zhuang, B. Gan, Targeting ferroptosis as a vulnerability in cancer, Nat. Rev. Cancer 22 (2022) 381–396, https://doi.org/10.1038/s41568-022-00459-0.
[8] S. Xu, Y. Feng, W. He, W. Xu, W. Xu, H. Yang, X. Li, Celastrol in metabolic diseases: progress and application prospects, Pharmacol. Res. 167 (2021) 105572, https://doi.org/10.1016/j.phrs.2021.105572.
[9] P. Luo, D. Liu, Q. Zhang, F. Yang, Y.K. Wong, F. Xia, J. Zhang, J. Chen, Y. Tian, C. Yang, L. Dai, H.M. Shen, J Wang, Celastrol induces ferroptosis in activated HSCs to ameliorate hepatic fibrosis via targeting peroxiredoxins and HO-1, Acta Pharm. Sin. B 12 (2022) 2300–2314, https://doi.org/10.1016/j.apsb.2021.12.007.
[10] M. Liu, Y. Fan, D. Li, B. Han, Y. Meng, F. Chen, T. Liu, Z. Song, Y. Han, L. Huang, Y. Chang, P. Cao, A. Nakai, K. Tan, Ferroptosis inducer erastin sensitizes NSCLC cells to celastrol through activation of the ROS-mitochondrial fission-mitophagy axis, Mol. Oncol. 15 (2021) 2084–2105, https://doi.org/10.1002/1878-0261.12936.
[11] Y.Z. Mazzu, J. Armenia, G. Chakraborty, Y. Yoshikawa, S.A. Coggins, S. Nandakumar, T.A. Gerke, M.M. Pomerantz, X. Qiu, H. Zhao, M. Atiq, N. Khan, K. Komura, G.M. Lee, S.W. Fine, C. Bell, E. O'Connor, H.W. Long, M.L. Freedman, B. Kim, P.W. Kantoff, A novel mechanism driving poor-prognosis prostate cancer: overexpression of the DNA repair gene, ribonucleotide reductase small subunit M2 (RRM2), Clin. Cancer Res. 25 (2019) 4480–4492, https://doi.org/10.1158/1078-0432.Ccr-18-4046.
[12] Z. Zuo, Z. Zhou, Y. Chang, Y. Liu, Y. Shen, Q. Li, L. Zhang, Ribonucleotide reductase M2 (RRM2): regulation, function and targeting strategy in human cancer, Genes Dis 11 (2024) 218–233, https://doi.org/10.1016/j.gendis.2022.11.022.
[13] P. Khan, J.A. Siddiqui, P.G. Kshirsagar, R.C. Venkata, S.K. Maurya, T. Mirzapoiazova, N. Perumal, S. Chaudhary, R.K. Kanchan, M. Fatima, M.A. Khan, A. U. Rehman, I. Lakshmanan, S. Mahapatra, G.A. Talmon, P. Kulkarni, A.K. Ganti, M. Jain, R. Salgia, S.K. Batra, M.W. Nasser, MicroRNA-1 attenuates the growth and metastasis of small cell lung cancer through CXCR4/FOXM1/RRM2 axis, Mol. Cancer 22 (2023) 1, https://doi.org/10.1186/s12943-022-01695-6.
[14] J. Tan, W. Wang, X. Liu, J. Xu, Y. Che, Y. Liu, J. Hu, L. Hu, J. Li, Q. Zhou, C11orf54 promotes DNA repair via blocking CMA-mediated degradation of HIF1A, Commun. Biol. 6 (2023) 606, https://doi.org/10.1038/s42003-023-04957-1.
[15] H.F. Yu, Z.Q. Yang, M.Y. Xu, J.C. Huang, Z.P. Yue, B. Guo, Yap is essential for uterine decidualization through Rrm2/GSH/ROS pathway in response to Bmp2, Int. J. Biol. Sci. 18 (2022) 2261–2276, https://doi.org/10.7150/ijbs.67756.
[16] D. Mossmann, S. Park, M.N. Hall, mTOR signalling and cellular metabolism are mutual determinants in cancer, Nat. Rev. Cancer 18 (2018) 744–757, https://doi.org/10.1038/s41568-018-0074-8.
[17] Z. Ye, Q. Zhuo, Q. Hu, X. Xu, L. Mengqi, Z. Zhang, W. Xu, W. Liu, G. Fan, Y. Qin, X. Yu, S. Ji, FBW7-NRA41-SCD1 axis synchronously regulates apoptosis and ferroptosis in pancreatic cancer cells, Redox Biol. 38 (2021) 101807, https://doi.org/10.1016/j.redox.2020.101807.
[18] C. Zhang, X. Liu, S. Jin, Y. Chen, R. Guo, Ferroptosis in cancer therapy: a novel approach to reversing drug resistance, Mol. Cancer 21 (2022) 47, https://doi.org/10.1186/s12943-022-01530-y.

[19] H. Wang, X. Liu, X. Yan, Y. Du, F. Pu, J. Ren, X. Qu, An ATPase-Mimicking MXene nanozyme pharmacologically breaks the ironclad defense system for ferroptosis cancer therapy, Biomaterials 307 (2024) 122523, https://doi.org/10.1016/j.biomaterials.2024.122523.
[20] X. Liu, P. Zhao, X. Wang, L. Wang, Y. Zhu, Y. Song, W. Gao, Celastrol mediates autophagy and apoptosis via the ROS/JNK and Akt/mTOR signaling pathways in glioma cells, J. Exp. Clin. Cancer Res. 38 (2019) 184, https://doi.org/10.1186/s13046-019-1173-4.
[21] X. Yu, X. Meng, M. Xu, X. Zhang, Y. Zhang, G. Ding, S. Huang, A. Zhang, Z. Jia, Celastrol ameliorates cisplatin nephrotoxicity by inhibiting NF-κB and improving mitochondrial function, EBioMedicine 36 (2018) 266–280, https://doi.org/10.1016/j.ebiom.2018.09.031.
[22] X. Chen, Y. Zhao, W. Luo, S. Chen, F. Lin, X. Zhang, S. Fan, X. Shen, Y. Wang, G. Liang, Celastrol induces ROS-mediated apoptosis via directly targeting peroxiredoxin-2 in gastric cancer cells, Theranostics 10 (2020) 10290–10308, https://doi.org/10.7150/thno.46728.
[23] J. Bian, Y. Ding, S. Wang, Y. Jiang, M. Wang, K. Wei, L. Si, X. Zhao, Y. Shao, Celastrol confers ferroptosis resistance via AKT/GSK3β signaling in high-fat diet-induced cardiac injury, Free Radic. Biol. Med. 200 (2023) 36–46, https://doi.org/10.1016/j.freeradbiomed.2023.03.004.
[24] Y. Zhan, L. Jiang, X. Jin, S. Ying, Z. Wu, L. Wang, W. Yu, J. Tong, L. Zhang, Y. Lou, Y. Qiu, Inhibiting RRM2 to enhance the anticancer activity of chemotherapy, Biomed. Pharmacother. 133 (2021) 110996, https://doi.org/10.1016/j.biopha.2020.110996.
[25] W. Xiong, B. Zhang, H. Yu, L. Zhu, L. Yi, X. Jin, RRM2 regulates sensitivity to Sunitinib and PD-1 blockade in renal cancer by stabilizing ANXA1 and activating the AKT pathway, Adv. Sci. 8 (2021) e2100881, https://doi.org/10.1002/advs.202100881.
[26] W.X. Chen, L.G. Yang, L.Y. Xu, L. Cheng, Q. Qian, L. Sun, Y.L. Zhu, Bioinformatics analysis revealing prognostic significance of RRM2 gene in breast cancer, Biosci. Rep. 39 (2019), https://doi.org/10.1042/bsr20182062.
[27] H. Xu, H. Zhao, C. Ding, D. Jiang, Z. Zhao, Y. Li, X. Ding, J. Gao, H. Zhou, C. Luo, G. Chen, A. Zhang, Y. Xu, H. Zhang, Celastrol suppresses colorectal cancer via covalent targeting peroxiredoxin 1, Signal Transduct. Targeted Ther. 8 (2023) 51, https://doi.org/10.1038/s41392-022-01231-4.
[28] C. Kun-Ming, C. Chih-Hsien, L. Chen-Fang, W. Ting-Jung, C. Hong-Shiue, L. Wei-Chen, Potential anticancer effect of celastrol on hepatocellular carcinoma by suppressing CXCR4-related signal and impeding tumor growth in vivo, Arch. Med. Res. 51 (2020) 297–302, https://doi.org/10.1016/j.arcmed.2020.03.001.